DETECTION AND ANALYSIS TECHNIQUES FOR OPTICAL TELESCOPE DATA AND MACHINE LEARNING APPLICATIONS

Corbin Cruz[(1)], Brent Buckalew[(1)], Jarod Melo[(1)], Mark Lambert[(1)], and Alyssa Manis[(2)]

[(1)] Amentum Services, Inc., NASA Johnson Space Center, Mail Code XI5-9E, 2101 NASA Parkway, Houston, TX 77058, USA
[(2)] NASA Orbital Debris Program Office, NASA Johnson Space Center, Mail Code XI5-9E, 2101 NASA Parkway, Houston, TX 77058, USA

ABSTRACT

The Eugene Stansbery-Meter Class Autonomous Telescope (ES-MCAT) is NASA's primary sensor for surveying small debris in geosynchronous earth orbit (GEO) and provides data for updating the NASA Orbital Debris Engineering Model (ORDEM). Data from 2020 to 2023 have been analyzed for use in supporting ORDEM 4.0 development. This ES-MCAT data set was compared with previously collected GEO survey data that used the Michigan Orbital Debris Survey Telescope (MODEST) to assess the evolving orbital debris environment and new insights that could be gained with updated survey methods and analysis techniques.

New methodologies in filtering detected objects for all GEO surveys and refinements of previous GEO breakup knowledge were investigated. The historical data are further compared to 2023 data analyzed using various detection techniques, including the introduction of machine learning (ML) to help detect orbital debris in optical images. The ML model uses the "You Only Look Once" version 9 (YOLO-v9) architecture and was trained on both simulated objects and objects detected during the 2023 GEO survey. This model improves detection completeness for faint and trailed objects when compared to previous software models. Nevertheless, limitations exist when dealing with a larger variety of object morphologies in astronomical images. Combining the previous software's detections with the new ML model increases the overall detection rate, including detecting objects too faint during manual review of data.

This paper presents an overview of the ES-MCAT GEO survey strategies; a comparison of data collected with ES-MCAT and MODEST; and the results of different detection methods, including manual review and ML. Applications to building and validating ORDEM are also discussed.

INTRODUCTION

The Eugene Stansbery-Meter Class Autonomous Telescope (ES-MCAT) is used by the NASA Orbital Debris Program Office (ODPO) to observe orbital debris in geosynchronous orbit (GEO), and these data are utilized to build and validate NASA's Orbital Debris Engineering Model (ORDEM). ES-MCAT completed its first GEO survey during 2020-2022 and began its second GEO survey in 2023 [1]. The pointing strategy created for the first GEO survey conducted by ES-MCAT was updated for the second GEO survey based on weather trends, Moon position, and galactic plane position. Prior to ES-MCAT's deployment, the ODPO also used the Michigan Orbital Debris Survey Telescope (MODEST) to collect GEO survey data during the years 2004-2006, 2007-2009, and 2013-2014 [2, 3, 4]. The data from the surveys conducted by these two telescopes were analyzed and compared to understand how improved survey methods, updated processing techniques, and a new observatory would impact the GEO survey results. In the process of analyzing data from the two telescopes and integration of data into ORDEM, methods to filter detections were implemented based on more recent target detections to better ensure that data only involves GEO debris.

To aid with future analyses of GEO survey data from ES-MCAT, the ODPO is also investigating the feasibility of machine learning (ML) to process large data sets for efficiency and minimize human-in-the-loop processes. ES-MCAT surveys involve large amounts of complex data and are prime candidates for ML applications. Machine learning is a type of artificial intelligence where a model learns from training data to identify patterns in new data. In the case of computer vision, ML is used to adjust the parameters of a convolutional neural network (CNN), which scans over an image so it can identify specific objects that are present in the training data.

This paper provides an overview of ES-MCAT GEO survey strategies, including updates made from the first to the second GEO survey; a summary of data collected during the first and second ES-MCAT GEO surveys and comparisons to historical MODEST data; and a discussion of performance of ML models implemented with ES-MCAT data.

Proc. 9th European Conference on Space Debris, Bonn, Germany, 1–4 April 2025, published by the ESA Space Debris Office
Editors: S. Lemmens, T. Flohrer & F. Schmitz, (http://conference.sdo.esoc.esa.int, April 2025)

SURVEY STRATEGIES

The goal of the ES-MCAT surveys were to optimize sampling of GEO objects within a region of interest (ROI), with an expected value (EVAL) of 0.3 or greater. The EVAL gives the probability of detecting an object in a specific orbit while at a given field of view and time. This ROI is defined with inclination (INC) and right ascension of the ascending node (RAAN) in INC·cos(RAAN) and INC·sin(RAAN) space, centered at 7.5°, 0°, with a radius of 15° [5]. ES-MCAT's GEO survey built upon the surveys from MODEST where observations were conducted near new moon and coverage gaps were filled in with statistical sampling. The ROI is shown in Fig. 1 along with the coverage of ES-MCAT's first GEO survey, with EVALs shown greater than 0.3 and 0.2.

A pointing strategy was developed for ES-MCAT's first GEO survey to cover this ROI, as uniformly as possible, within the GEO debris belt over two years, while also allowing for certain lapses in coverage. Each night, a series of images were taken at two right ascensions (RA) and two declinations (Dec), with one of RA and Dec pointing during each half of an 8-hour observing period. This was repeated for 24 more nights with decreasing RAs and Decs that trailed and lead the approximate center of Earth's shadow by 15 degrees, creating one cycle that spanned a portion of the GEO belt. These cycles repeated 13 more times and encompassed 350 nights, approximately one year. These cycles could be repeated indefinitely, while ensuring the GEO belt bounds were updated to reflect the perturbation and corresponding evolution of GEO objects' orbits. This pattern is similar to MODEST's GEO survey approach where one cycle appears as two vertical lines in RA/Dec space, following Earth's shadow [2, 3]. The resulting ES-MCAT planned pointings are shown in Fig. 2, descriptively named the "Candy-Cane Method," along with the actual pointings from ES-MCAT's first GEO survey.

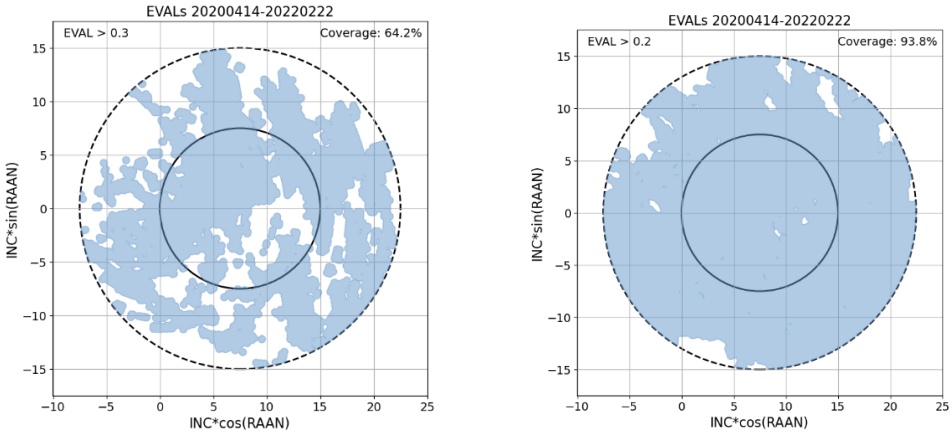

Figure 1. (left) ROI coverage plot taken from the first ES-MCAT GEO survey showing regions that exceeded an EVAL of 0.3. (right) ROI coverage plot taken from the first ES-MCAT GEO survey showing regions that exceeded an EVAL of 0.2. Both plot titles are in the format YYYYMMDD.

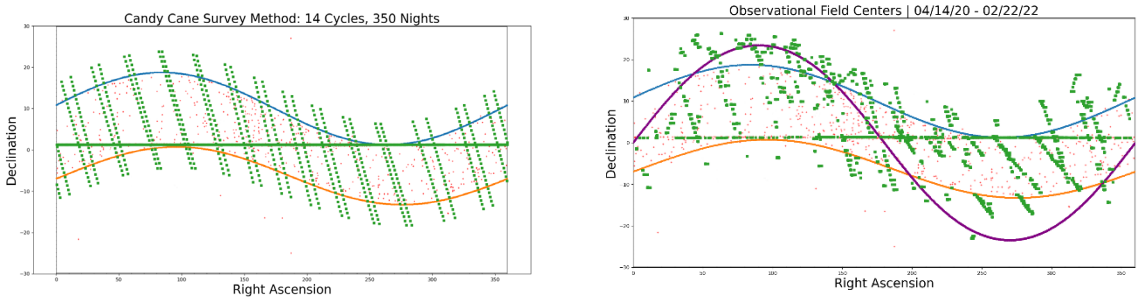

Figure 2. (left) The pointing strategy implemented in ES-MCAT's first GEO survey in RA/Dec space for 14 cycles, or 350 observational nights. Green squares represent planned field centers for each night, red markers represent cataloged GEO objects from January 2021, and the blue and orange curve represent the approximate upper and lower bounds of the GEO belt. (right) Actual field center pointings from ES-MCAT's first GEO survey, with an additional purple curve representing the path of Earth's shadow.

Field center differences between the planned pointings and the actual pointings can be attributed to weather downtime, unplanned maintenance, and Moon brightness preventing useful observations. These effects also impacted the overall coverage and will be discussed below. The original survey method allowed for manual pointings, which enabled focused observations for reducing large coverage gaps in the ROI. The survey method for ES-MCAT's second GEO survey was improved upon in several ways. First, to minimize overexposure from the moon, an area encompassing a radius of 20° around the Moon is implemented for avoidance, with pointing scheduled either higher or lower in Dec. Second, an approximation of the galactic plane's position in RA/Dec space with an additional boundary of 7.5° is implemented for an avoidance zone. The numerous star trails, which make it difficult to detect faint objects and ultimately increases processing time. Understanding the weather behavior for Ascension Island is critical for maximizing available observation days. For example, best photometric days occur in March with least photometric/bad weather days in September and October [6]. To address these gaps in coverage due to seasonal effects, a wider declination is used for poor conditions (10 days per cycle versus the nominal 25 days). The end result with all three of these optimized field pointings are shown in Fig 3.

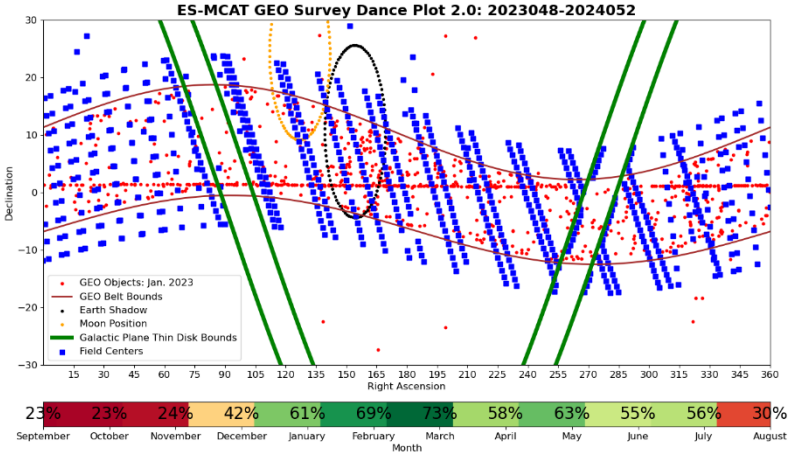

Figure 3. Chart showing planned pointings/dance plot for the second GEO survey in RA/Dec space; blue squares represent the pointings for each night. Also plotted are the galactic plane thin disk bounds (green curves), cataloged GEO objects propagated to January 2023 (red dots), upper and lower bounds of the GEO belt (red curves), and nightly availability by month (color bar at bottom). Earth's shadow (±10°) and the Moon's position (±10°) for 21 February 2024 are also depicted by the black and yellow ellipses, respectively.

To understand how this updated pointing strategy affects coverage over the ROI, the planned field centers were processed through an in-house developed ODPO program known as Tie-Dye. This program simulates orbits with various INCs and RAANs based on the time of observation and produces predicted EVALs for the upcoming survey along with previous instances of this program being utilized for telescopic measurements with MODEST [7]. Tie-Dye was run for an ideal survey with no effects from weather along with an average survey with the nightly observation availability specified in Fig. 6. The effect is that certain regions of the Tie-Dye plot lose coverage, causing regions of the plot to show smaller total EVALs. These two scenarios are depicted in the ROIs in Fig. 4.

Despite lower EVALs due to predicted weather events in the right-hand chart of Fig. 4, the minimum EVAL within the ROI is still at least 0.3, which meets the goal of the GEO survey. A Titan Transtage breakup that occurred in 2019 (International Designator 1976-023F, U.S. Satellite Catalog Number 8751), modeled with the NASA Standard Satellite Breakup Model (SSBM) and propagated to December 2020, is depicted in the charts with black dots. Also plotted are the modeled GEO objects from ORDEM 3.1, which are propagated to the end of 2019, marked with gray dots.

DATA PROCESSING

Detection of orbital debris in optical images generally involves humans manually reviewing images, along with the use of software algorithms to analyze images and identify detections that correspond to Earth-orbiting objects. ES-MCAT data are processed with manual review of images to detect objects and use the Observatory Control System (OCS) software to photometrically and astrometrically calibrate detected objects in a series of images [8]. Detections with MODEST data utilized a processing software based on the Image Reduction and Analysis Facility (IRAF) code developed by the National Optical Astronomy Observatories (NOAO) for data reduction in addition to periodic manual review for comparison with the debris finder program [2]. For both MODEST and ES-MCAT surveys, after image reduction was completed and detected objects were identified, objects were correlated with the Space Surveillance Network (SSN) catalog available from SpaceTrack.org and assigned as a correlated target (CT), which includes both intact objects and large orbital debris, or an uncorrelated target (UCT).

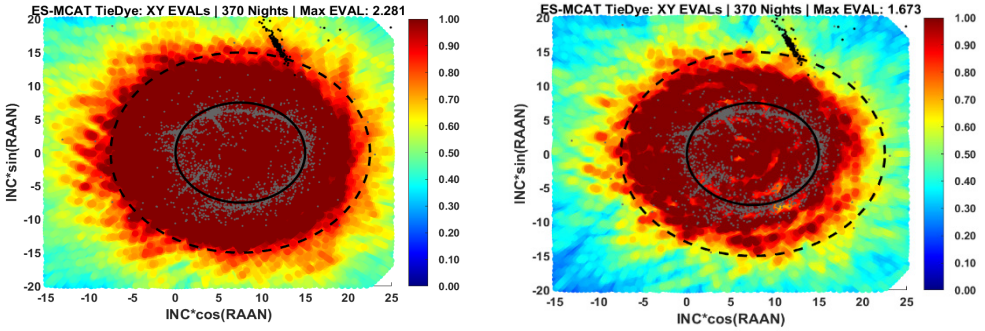

*Figure 4. ROI plots of coverage resulting from the pointing strategy of the second GEO survey in INC*cos(RAAN), INC*sin(RAAN) space. The ROI are indicated by the dashed black lines, modeled GEO debris (propagated to late 2020) are shown with gray dots, and a modeled 2019 Titan Transtage breakup (propagated to late 2020) is shown with black dots. The EVALs within the plots are shown by a range of colors, indicated on the color bar on the right-hand side of each plot. The plot on the left utilized an ideal survey with no weather events, while the plot on the right removed certain field centers based on monthly availability (see Figure 6).*

GEO SURVEY RESULTS

The following will provide analyses conducted on the correlated data from the first and second ES-MCAT GEO surveys, consisting of 1,895 total objects.

Of the total 1078 objects found by manual review during the first ES-MCAT GEO survey, 165 objects were categorized as UCTs, and 913 were categorized as CTs. During the first three months of the second GEO survey, 817 objects were detected with 423 categorized as CTs and 394 as UCTs, surpassing those detected in the first GEO survey. The primary mirror was recoated between the first and second GEO surveys, so the greater number of UCTs detected during a shorter time span is likely owed to the newly recoated mirror and better detection capabilities of the system. The detections from the first and second surveys, along with the modeled GEO objects and Titan 2019 breakup (propagated to late 2020), are also presented in the ROI plots in Fig. 5.

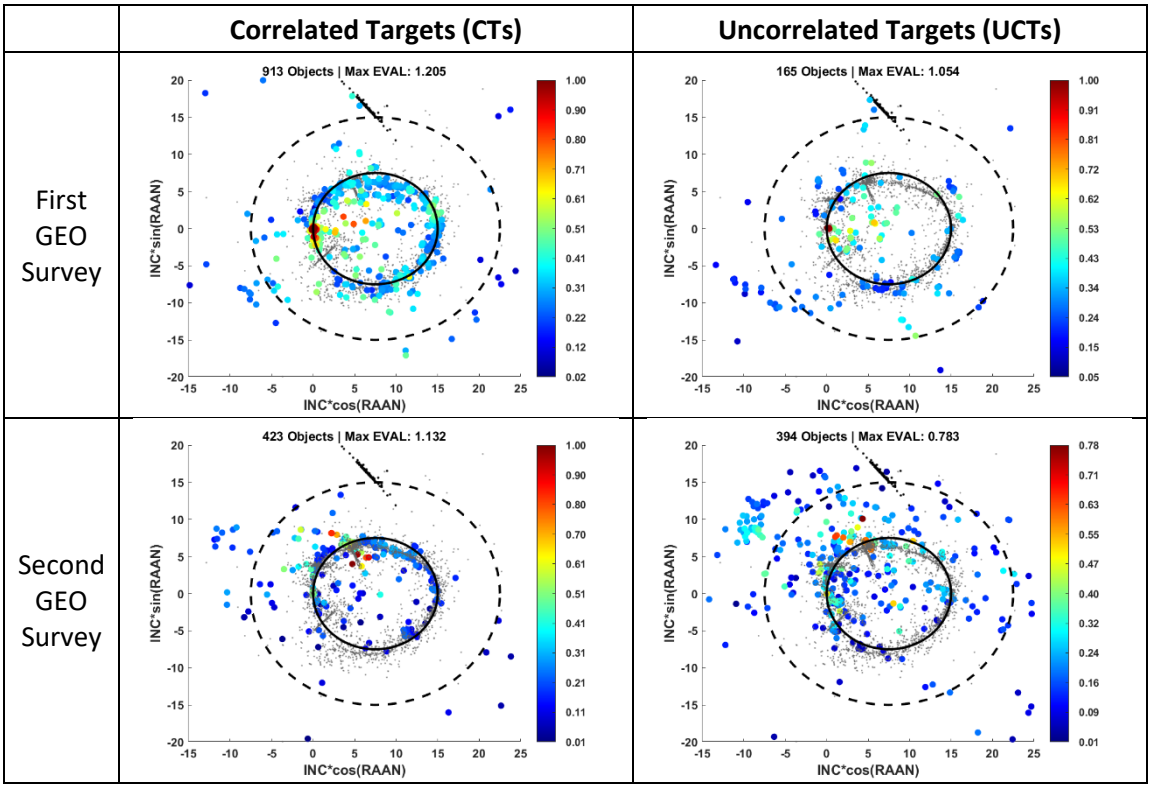

*Figure 5. ROI plots of CT and UCT detections from the first and second ES-MCAT GEO surveys in INC*cos(RAAN), INC*sin(RAAN) space, similar to those in Fig. 4.*

To further characterize the detected objects in the two surveys, the absolute magnitudes of each object were calculated from the measured apparent magnitudes and calibrated to GEO altitudes and plotted in histograms for ES-MCAT and MODEST surveys, shown in Fig. 6.

The number of detections in the second ES-MCAT GEO survey (ES-MCAT 23 Manual) increases up to approximately 18th magnitude, as opposed to the drop-off after approximately 17th magnitude seen in the first GEO

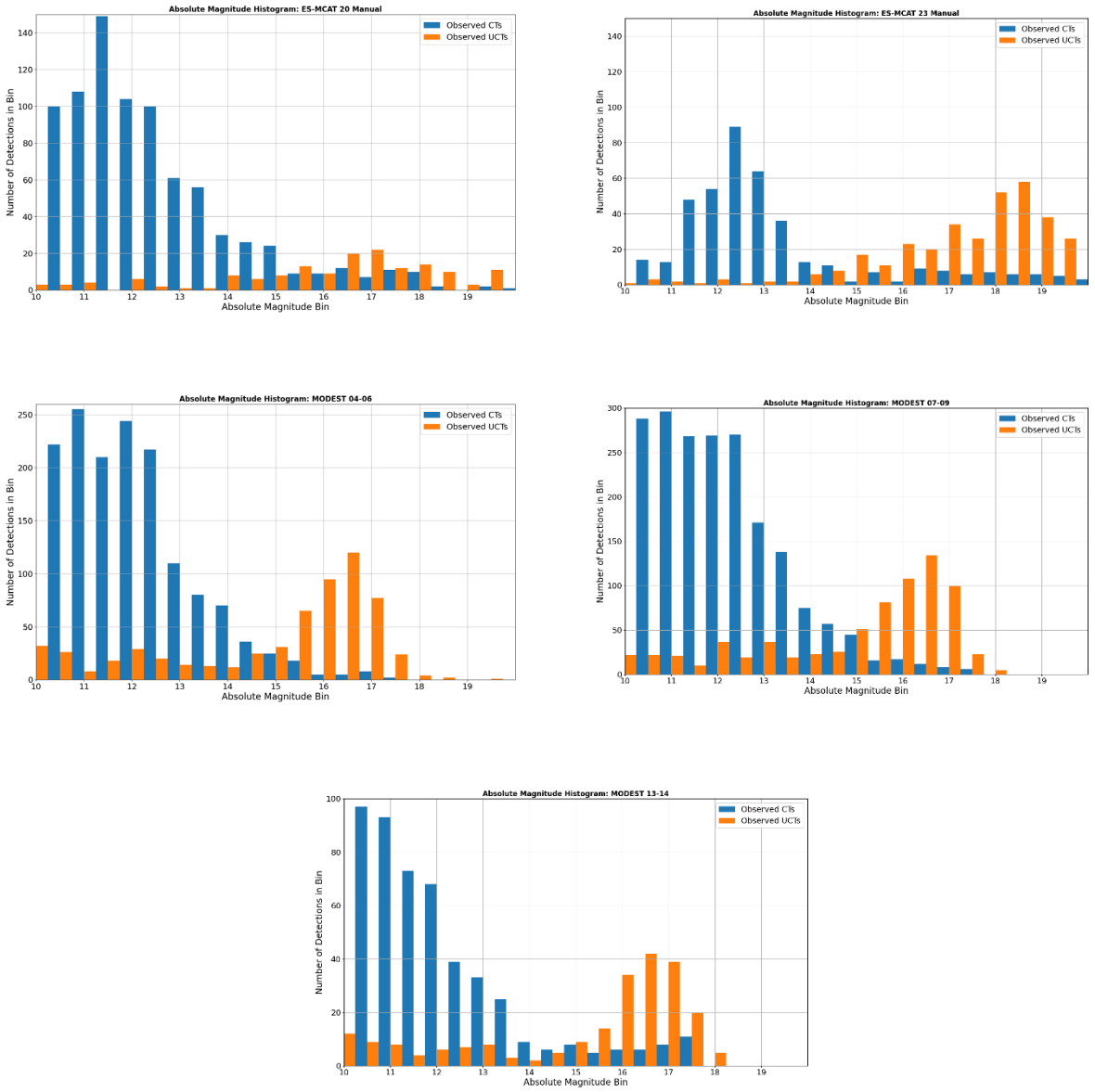

Figure 6. Histograms of detected objects (CTs and UCTs), binned by absolute magnitude. Separate plots show the different surveys conducted: the first two ES-MCAT GEO surveys, ES-MCAT 20 Manual and ES-MCAT 23 Manual, respectively, and the three MODEST GEO surveys. Note the different y-axis ranges between the plots.

survey (ES-MCAT 20 Manual) and approximately 16.5 magnitude seen in the MODEST datasets. This roll-off is due to the recoated primary mirror and more focused survey strategy discussed above. An increase of dimmer objects detected correlates to a higher probability of small debris (<30 cm) being found.

Data on small orbital debris in GEO below the size threshold of the SSN catalog is of primary interest for the purposes of ORDEM. A data filter is applied to focus on GEO debris, thus removing larger objects not of interest or objects with rates outside of GEO that may appear as GEO debris during the short time arc. Before filtering, the detections from all surveys are propagated to a common epoch, chosen here to be December 2020. The first filter that is implemented on the telescopic measurement data is based on the type of observed objects. Cataloged breakup debris objects are identified in the CT object data set based on their International Designators and SSNs, and up to 2023, these include 8 GEO breakups: Ekran 2 (1978); Ekran 4 (1981); Ekran 9 (1983); Titan 3C (1992, 2018, 2019); Briz-M (2016); and Beidou (2016) [9]. At the end of the last MODEST survey in 2013-2014, only 4 known GEO breakups had occurred (Ekran 2 (1978), Ekran 4 (1981), Ekran 9 (1983), and a Titan 3C rocket body (1992). Next, UCT objects are filtered by size, with the lower size limit being 25 cm and the upper size limit being 1.25 m. While the detection capabilities and data completeness of MODEST was 30 cm, ES-MCAT's capabilities allow for the lower size limit to be lowered to 25 cm, and the lower size limit for all datasets were decreased for comparison. These sizes are calculated from the NASA Optical Size Estimation Model (OSEM). Finally, the UCTs are filtered based on the stable Laplacian plane for GEO objects to better ensure that UCTs are indeed GEO objects instead of GEO transfer (GTO) or MEO objects. The effects of these filters on the observed objects in the ROI plots (which approximate the stable Laplacian plane) are indicated in Fig. 7 for ES-MCAT and MODEST survey data.

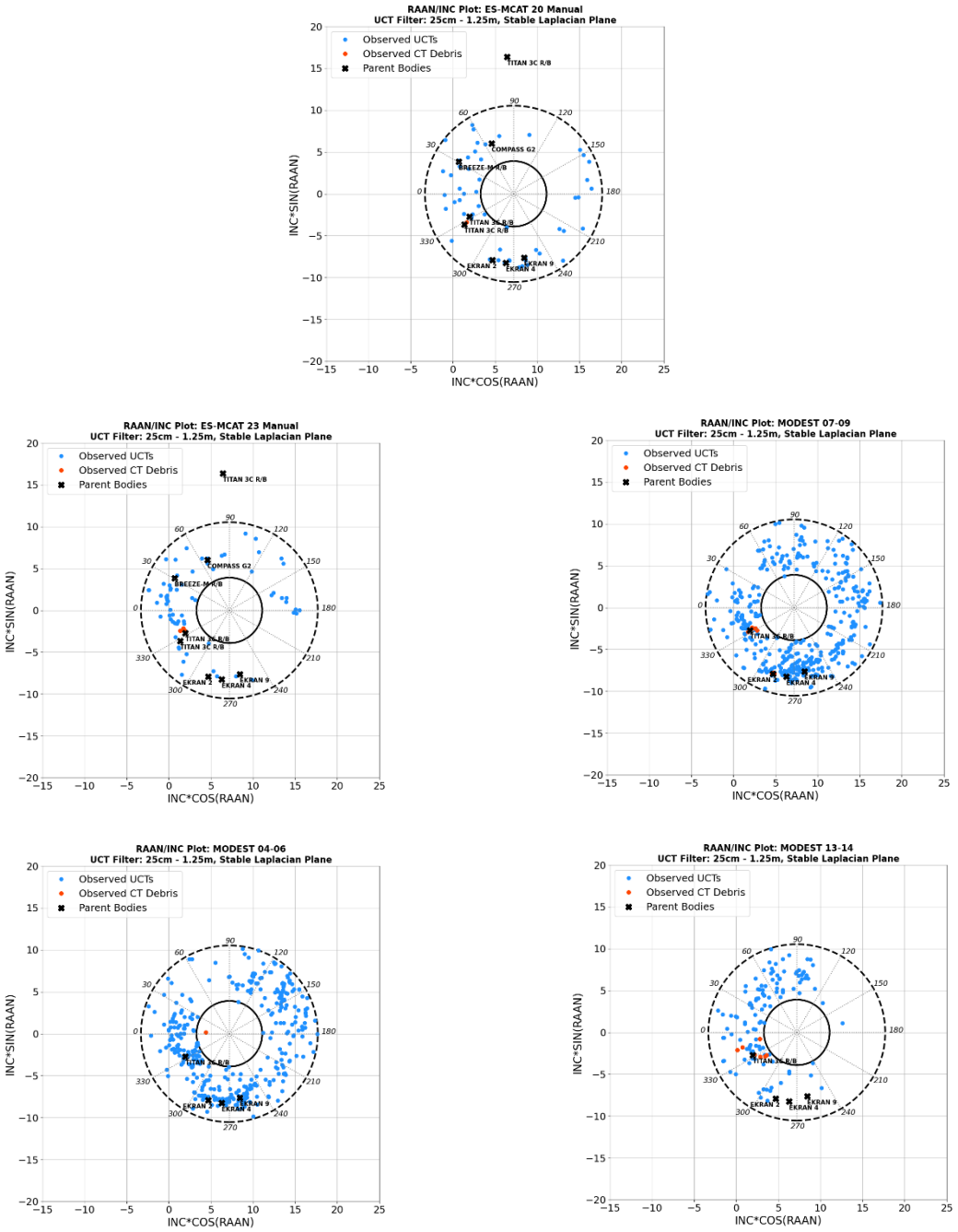

*Figure 7. ROI plots of filtered detections from the first and second GEO surveys in INC*cos(RAAN), INC*sin(RAAN) space, with the order of surveys identical to Fig. 6. The dashed and solid circles represent the ROI, which approximates the stable Laplacian plane region. Detections are represented by dots, and modeled parent bodies (propagated to late 2020) are represented by X's. The dashed "pie wedges" represent the "clock angles" in the ROI from the left and moving clockwise.*

These polar plots indicate where objects exist in GEO with the additional comparison to breakup parent bodies. While there were a large number of detections during the surveys, the effect of the filters reduces these numbers, especially with the ES-MCAT data. Manual review with ES-MCAT allowed for the additional detections of GTO objects and MEO objects, which were not included in these plots. There were also a larger number of detections in the MODEST 04-06 and 07-09 GEO surveys when compared to ES-MCAT 20 due to the limited detection capabilities of the ES-MCAT observatory over the first GEO survey. The reason for this was because of the degraded mirror coating and the inability to travel to clean the mirror in addition to weather downtime and unplanned maintenance at the observatory. There were also fewer detections in the ES-MCAT 23 data set due to the fact that it only spans over 3 months of observational data. The pie wedges seen are "clock angles," defined as an angle in the Cartesian coordinates of INC*cos(RAAN), INC*sin(RAAN) where 0° clock angle is defined by a vector originating at (7.5°,0°) and pointing in the (0°,0°) direction, and the angle increases moving clockwise. These allow for understanding completeness and number of detections within certain orbits. These are investigated further in the Fig. 8 with the uncertainties in detections included.

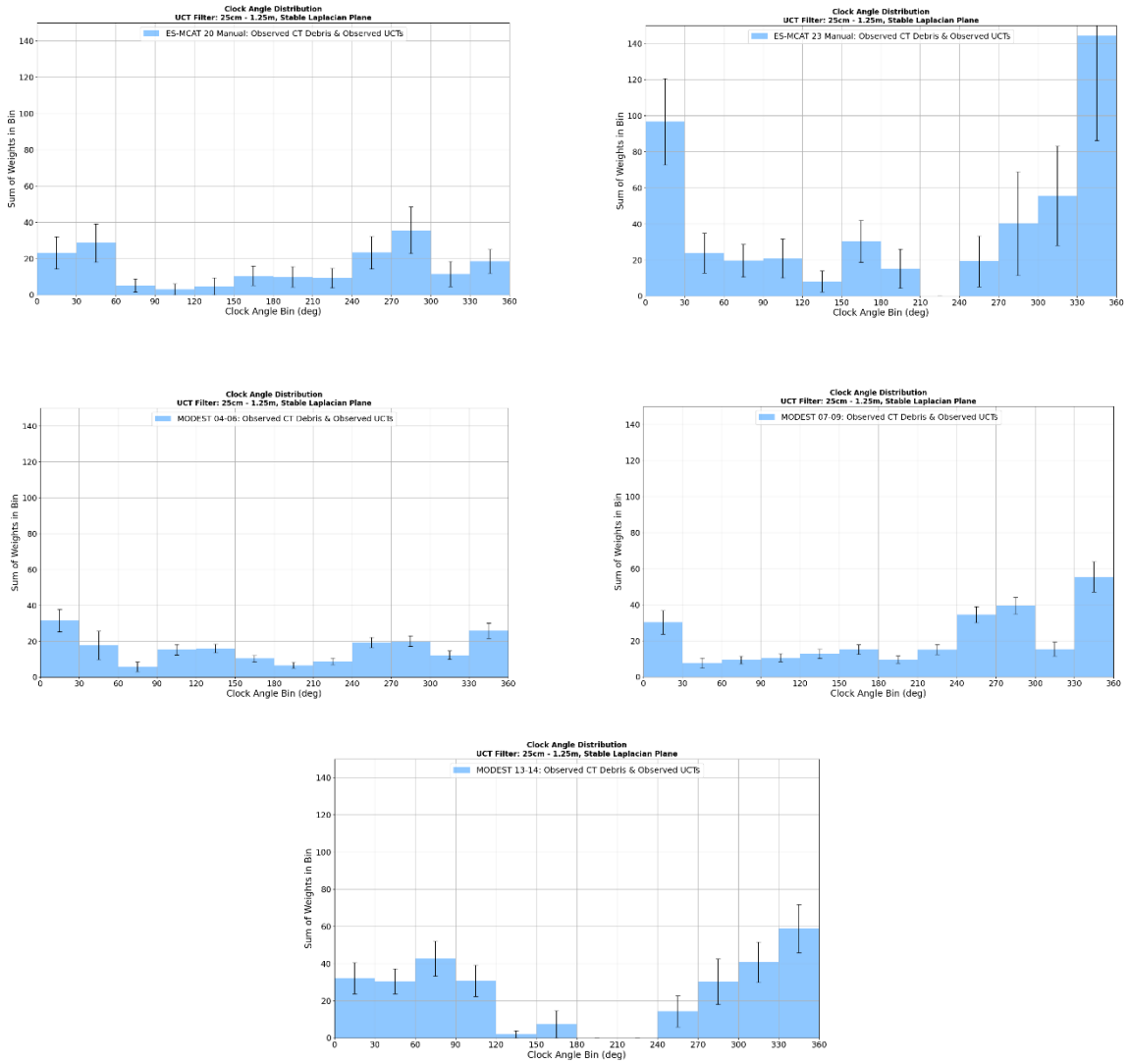

Figure 8. Histograms of the sum of weights (WTs) of filtered detected objects in each clock angle bin, with the order of surveys identical to Figs. 6 and 7. The Poisson uncertainties of the filtered detections are shown. Note the different y-axis ranges between the plots.

The detections in each clock angle bin are added based on their WT given to each detection. The WTs are the inverse of the EVALs discussed in the Survey Strategies section. The sum of detected object WTs in each clock angle bin are generally higher between 240-330 degrees while they are lower between 90-240 degrees. This is true for both ES-MCAT and MODEST surveys and mirrors the detections in Fig. 7. This could be attributed to the amount of time that a certain orbital regime was surveyed when compared to others, the telescope's ability to detect dim objects that are likely small debris, or a relatively lower proportion of debris in those orbital regions. While the clock angle distribution plots are a good way to understand where orbital debris may lie in space, cumulative size plots aid in understanding the distribution of objects in terms of their estimated size, shown in Fig. 9.

By including the 8 modeled GEO breakups, the measurement data for each survey can be compared to the models. In all cases, the cumulative size curves generally follow the curve for 8 modeled GEO breakups. Since only 4 known GEO breakups occurred before the years covered by the MODEST surveys, the 8 modeled GEO breakups curve is higher than the MODEST 04-06 data curve below approximately 80 cm; however, it is comparable to the MODEST 07-09 and 13-14 data curves at these smaller sizes, which may indicate more GEO breakups occurred prior to these time frames than have been confirmed.

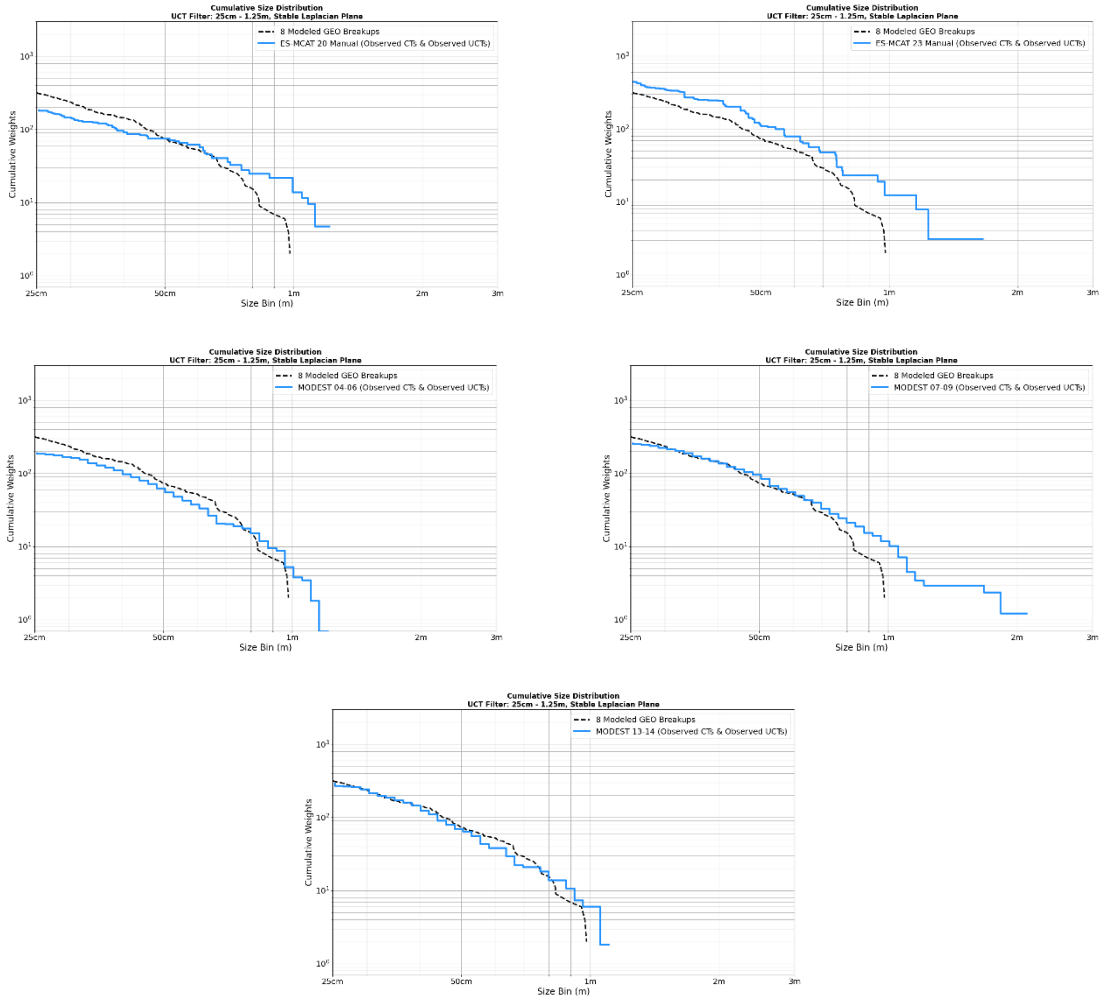

Figure 9. Cumulative WTs curves of filtered detected objects with respect to the objects' estimated sizes in log-log space, with the order of surveys identical to Figs. 6, 7, and 8. The filtered survey detections cumulative weights are represented by the blue line, the 8 modeled GEO breakups curve is represented by the black dashed line.

While the ES-MCAT 2023 survey only included 3 months of data, its curve is higher than the modeled curve by approximately a factor of 1.5 up to approximately 80 cm. This could indicate additional, unknown GEO breakups that have occurred since the previous surveys or that occurred before the previous surveys but were not captured in the earlier data sets and is likely attributed to the new mirror coating and enhanced detection capabilities.

MACHINE LEARNING METHODOLOGY

Recently, ML models have been developed to assess performance for detecting debris with ES-MCAT as compared to manual review and previous software detection methods in an effort to expand the data sets available for analysis. A predictive ML model is trained on data representative of telescope detections. For ES-MCAT GEO survey observations, detected objects appear as point sources or short streaks and stars appear as long streaks (see Fig. 10). A limitation of using only real object detections is that the number of objects found with ES-MCAT over its survey durations is on the order of 100 objects, while an ML model would benefit from thousands of objects to train a robust and accurate object detection model. To expand on the data set of real detections and provide a large set of training data, the simulation capabilities of OCS were used. These can randomly generate any number of objects onto an image with random assigned streak lengths and magnitudes [10]. OCS simulations were run to generate 10 objects with any streak length between 0 and 4 arcseconds, random orientation, and a magnitude between 8 and 21. In total, OCS generated 5530 simulated objects. To ensure the model was trained on visible/real objects, the simulated objects were reviewed by humans. Since some simulated objects were too faint to be detected by humans or below the noise floor, only 4231 were available for model training and validation. Fig. 10 shows a typical image with simulated objects.

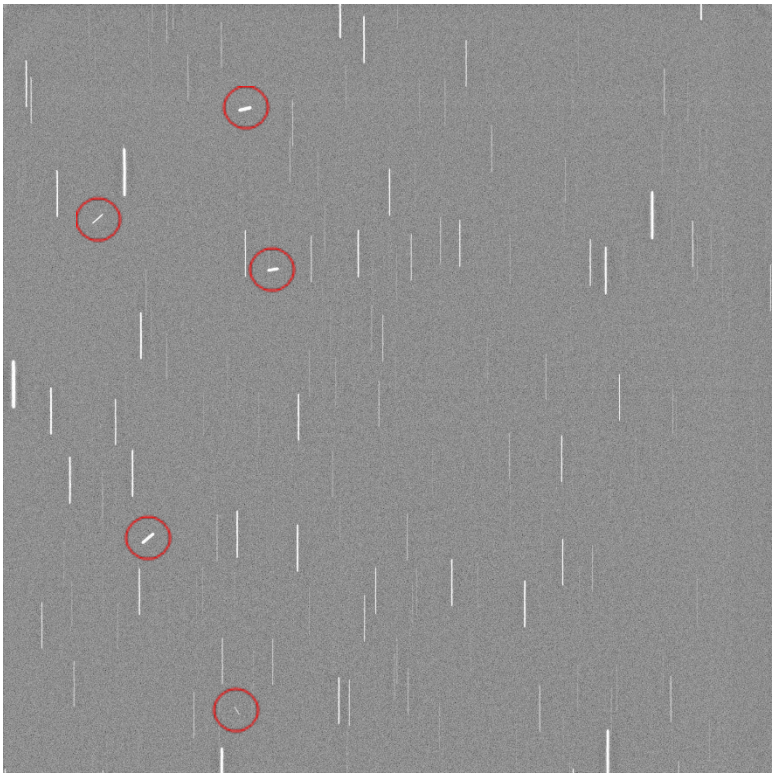

Figure 10. An example of a typical simulated object image used for the training model. The underlying image was taken using ES-MCAT on 8 February 2023. The long, vertically streaked objects are star trails. Of the 10 simulated objects used in the image, 5 are visible and circled in red, while the remaining 5 were too faint for human detection.

The "You Only Look Once" version 9 (YOLOv9) architecture was used to train the ML model with these simulated objects. YOLOv9 [11] is a convolutional neural network (CNN) architecture that has a near state-of-the-art accuracy while also remaining fast to run in both train and inference modes. The original 4096x4096 TIFF images from ES-MCAT are first tiled into 16 1024x1024 PNG tiles. This is necessary because the objects are small relative to the size of the image, so the images could not be significantly resized during training. This also enables tiles to be shuffled during training and allows the data set to fit in limited memory. The YOLOv9-C pretrained model was used for initialization. The model was trained with default hyperparameters with a batch size of 64 and image size of 1024. Once trained, the model can be run on new images for inference. With an RTX 5000 Ada laptop GPU, inference only takes 50 ms per tile, or 800 ms per full-size image. A typical detection of the ML model is given in Fig. 11.

Two ML models were constructed. The first model (termed streak model) relied solely on the simulated objects discussed above. A limitation of using only simulated objects is that the objects could have motions of 0-4". The random number generator rarely hits 0" and so the model was not trained on point sources, which are typical in actual images of station-kept GEO spacecraft. For images of the GEO belt, the streak model would not detect any of the station kept objects. Thus, a second model was generated (termed streak+point model) with the addition of 42 station-kept objects from ES-MCAT observations taken on 16 January 2024. Rather than being a binary object detector like the previous model, the streak+point model was trained to detect two classes: streaked objects "streaks" and point sources "points." These two classes were given different labels in training, which allowed the model to differentiate them and produce labeled outputs.

Both models were trained with default hyperparameters with the following changes. Image size was set to 1024. Flip up-down and flip left-right probabilities were both set to 0.5. Image scale was reduced to 0.1 to only allow for small amounts of resizing at train time (images would be randomly rescaled between 0.9x and 1.1x each epoch). Mosaicking and copy-paste augmentations were turned off. Below, we detail the results that the two ML models produced in comparison to the human-derived and OCS-derived results.

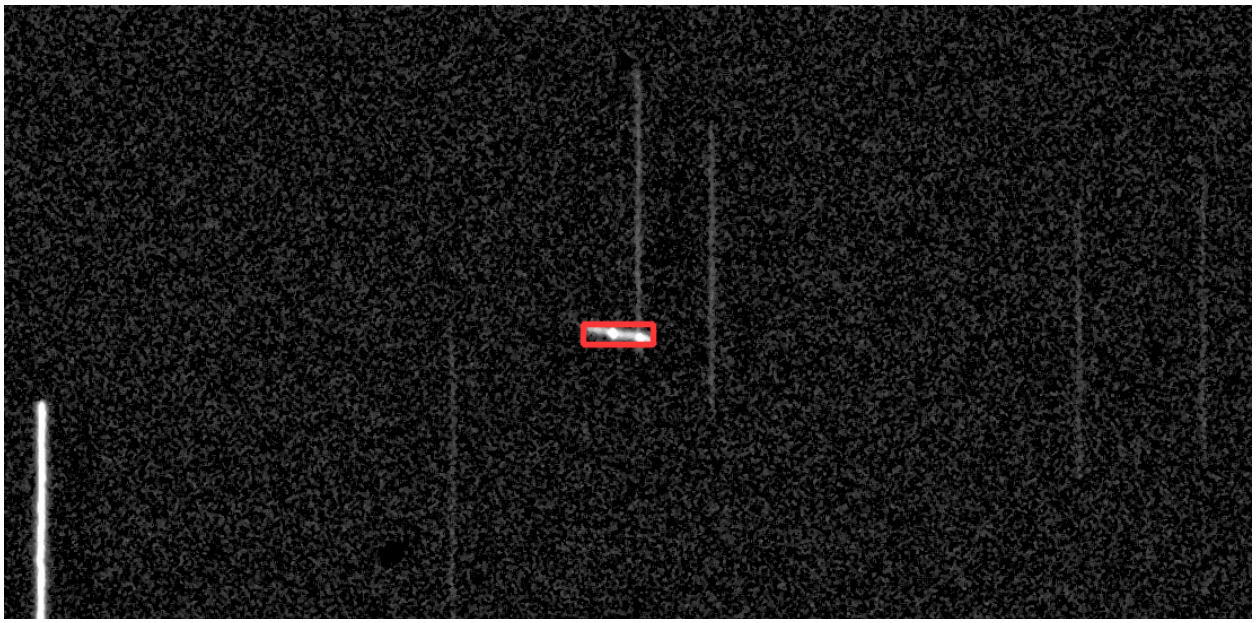

Figure 11. An example of a typical detection by the streak model. This object was detected in data obtained on 7 March 2023. This object appears in only 2 images and the model finds the object each time. While the simulated data used to train the model does not have streaks with bright nodules throughout, as with this detection, the machine model can still accurately detect them.

MACHINE LEARNING RESULTS

A comparison of the results using manual review of images, the OCS detection algorithm, and the streak model on GEO survey data from 16 January 2023 through 3 February 2023 is given in Tab. 1 below. With the streak model, 14 objects were discovered that were missed during manual review, a substantial improvement in identifying objects below the human detection threshold. Otherwise, the number of objects identified during manual review includes all objects detected by either the streak model or OCS, so that the total number of objects is the sum of the manual review number and the 14 faint objects. Even with these missed objects, manual review of the data still finds 96% of objects. The streak model finds 69% of the total objects in these data sets with the majority of missed objects being bright, overexposed point sources. Compared to OCS (45%), the streak model is a better detection method, but both computerized methods fall significantly below the manual review. If OCS and the streak model are combined (removing any overlap of detected objects to avoid double counting), the percentage of total objects detected rises to 86%, a significant improvement over using one method alone.

Table 1. Results from manual review, the OCS algorithm, and the streak model for GEO survey data from 2023.

Set Name	Number of Objects	Percent of Total
Manual review	301 / 315	96%
OCS	143 / 315	45%
ML streak model	218 / 315	69%
ML/OCS combined	270 / 315	86%
Total	315	--

With the addition of the streak+point model, we can see if classes have significantly improved the results, shown in Tab. 2. The ES-MCAT data used in this analysis runs from 17 January 2023 through 15 March 2023. Please note that 16 January 2023 data were not used because these data were used to create the streak+point model, and it was desired that the data sets in these two analyses are independent of one another. With these data sets, the streak model only found 4 objects that the human review missed.

Table 2. Results from manual review, the streak+point model, and the streak model for GEO survey data from 2023. The 199 objects for streak model include 4 objects that were missed during manual review.

Set Name	Number of Objects	Percent of Total
Manual review	296 / 300	95%
ML streak+point model	170 / 300	57%
ML streak model	199 / 300	66%
ML combined	232 / 300	77%
Total	300	--

For ES-MCAT data from 2 March 2024 to 15 March 2024, we ran both ML models, OCS, and manual review on this data set, with the results summarized in Tab. 3. The resulting percentages of manual review, the streak model, and OCS are similar at 100%, 69%, and 45% to the previous results.

Table 3. Results from manual review, the ML streak+point model, and the streak model for GEO survey data from 2023.

Set Name	Number of Objects	Percent of Total
Manual review	77 / 77	100%
ML streak+point model	50 / 77	65%
ML streak model	53 / 77	69%
OCS	35 / 77	45%
ML combined	65 / 77	84%
OCS+streak model	65 / 77	84%
All 3 software results	67 / 77	87%
Total	77	--

SUMMARY

With the completion of the first GEO survey with ES-MCAT, updates to the survey strategy were identified to improve the photometric and astrometric processing of the collected images along with improving coverage of the ROI. Data from the second ES-MCAT GEO survey in combination with the first and data from the MODEST surveys, included here, allow for a general understanding of changes to the GEO debris environment and how the ORDEM GEO population is developed. The effects of filtering methods to better ensure that only small debris is

counted in these populations were shown on the ROI/Laplacian Plane, clock angle bins, and cumulative size plots. Incoming data from the second ES-MCAT survey, although spanning only three months, adds new insights into the GEO debris population, especially with the addition of manual review and ML.

The fundamental takeaway from the ML study is that manual review still provides the best performance for detecting debris in the optical images. Due to eye fatigue or human error, however, the streak model finds objects that humans can miss. Nonetheless, the streak model could be paired with various combinations of other ML models that focus on point sources exclusively or the OCS software results to improve the overall software result. Ultimately, no software can replace the manual review entirely, but this analysis has shown the potential for ML to enhance results obtained with manual review. Additional model improvements can be attained by expanding the data set with additional images to improve the detection rates for objects underrepresented in the current simulated training data, or by building an ensemble of models. Analysis of performance of the streak and streak+point models is underway to understand limitations and opportunities for an improved ensemble.

REFERENCES

1. Cruz, L. C., et al. (2023). “The Completion of a Geosynchronous Earth Orbit Survey with the Eugene Stansbery-Meter Class Autonomous Telescope,” Second International Orbital Debris Conference, Sugar Land, Texas.
2. Abercromby, K. J., et al. (2010). “Michigan Orbital DEbris Survey Telescope Observations of the Geosynchronous Orbital Debris Environment, Observing Years: 2004-2006,” NASA/TP-2010-216129.
3. Abercromby, K. J., et al. (2011). “Michigan Orbital DEbris Survey Telescope Observations of the Geosynchronous Orbital Debris Environment, Observing Years: 2007–2009,” NASA/TP-2011-217350.
4. Kennedy, T., et al. (2022). “NASA Orbital Debris Engineering Model (ORDEM) 3.1: Model Verification and Validation,” NASA/TP-20220002309.
5. Cruz, C., et al. (2023). "Updates of the Eugene Stansbery-Meter Class Autonomous Telescope for Geosynchronous Orbit Survey Operations,” Orbital Debris Quarterly News, Vol. 27, Issue 1, pp. 4-5, March.
6. Lederer, S.M., et. al. (2019). “NASA’s Orbital Debris JAO/ES-MCAT Optical Telescope Facility on Ascension Island,” First International Orbital Debris Conference, Sugar Land, Texas.
7. Abercromby, K., et al. (2008). “A Summary of Five Years of Michigan Orbital Debris Survey Telescope (MODEST) Data,” IAC.
8. Hickson, P. (2019). “OCS: A Flexible Observatory Control System for Robotic Telescopes with Application to Detection and Characterization of Orbital Debris,” First International Orbital Debris Conference, Sugarland, TX.
9. Anz-Meador P. D., Opiela J. N., and Liou J.-C. (2022). “History of On-Orbit Satellite Fragmentations (16th ed.),” NASA TP-20220019160.
10. Hickson, P., et al. (2023). “Automated Detection and Analysis of Resident Space Objects with the 1.3-meter Eugene Stansbery-Meter Class Autonomous Telescope,” Second International Orbital Debris Conference, Sugarland, TX.
11. Wang, C.-Y., et al. (2024). Yolov9: Learning what you want to learn using programmable gradient information (arXiv:2402.13616). http://arxiv.org/abs/2402.13616 .